Rheinische Friedrich-Wilhelms-Universität Bonn

Advanced Laboratory Course

Performed on: April 4th - 5th, 2022

Submitted on: May 3, 2022

A249: Laser Gyroscope

Authors
Paarth Thakkar
Keito Watanabe

Tutor(s)
Thorsten Groh
Marc Vöhringer

Abstract

Contents

Chapter 1

Introduction

The rotation of the Earth has been investigated ever since the advent of calenders. The first measurements for the rotation of the Earth has been done by observing the apparent position of a fixed star, allowing the Mayans to obtain measurements with relative uncertainties of around 10^{-5} [1].

Today, the rotation of the Earth is measured using interferometry, where radio telescopes all around the world are linked to construct a very-long base-interferometer system (VBLI). Fig. 1.0.1 show the locations of all radio telescopes under the CONT17 campaign, a continuous VLBI session held for two weeks in 2017 [2]. The relative uncertainties that are obtained reach approximately 10^{-10}. Today, the rotation of the Earth is measured to be approximately $72.92\,\mu\text{rad}\,\text{s}^{-1}$ along its rotation axis [1].

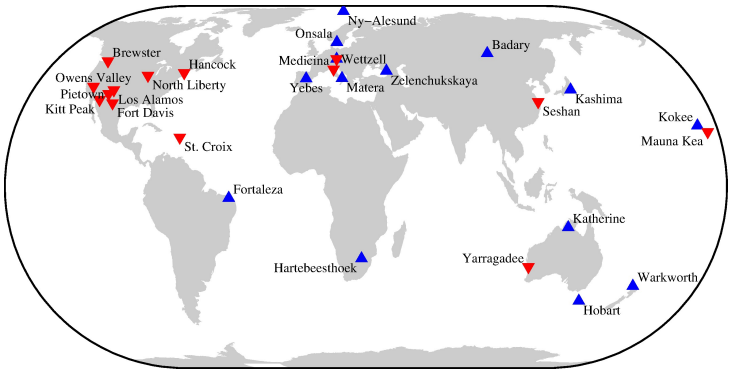

Figure 1.0.1: Radio telescopes used for CONT17. Both blue and red markers indicate legacy stations used for measurements in past sessions.

Determining the rotation of the Earth allows us to understand the vast phenomena that occur on Earth, including tidal breaking, seasonal variations, and the Chandler wobble, the nutation that occurs with Earth's rotation axis. Furthermore, climate change has a strong effect on the rotation rate as the melted ice from the polar ice caps gravitate towards the equator, increasing the angular momentum and thus the rotation period of Earth. This is shown to increase at a rate of $1.2\,\mu\text{s}$ per year [1].

While the VLBI can determine the rotation rate with high precision, due to the operation times the temporal resolution is low. As such, transient events such as earthquakes and tides cannot be resolved. As of such, laser gyroscopes have been employed to resolve such details. While it lacks in the long-term stability of VLBI, they have a temporal resolution of approximately an hour or less [3]. The G-ring at the German Fundamentalstation Wettzell is one of the best ring laser gyroscopes with a sensitivity of around $12\,\text{prad/s}/\sqrt{\text{Hz}}$ [1]. See Fig. 1.0.2 for an image and the setup of the G-Ring gyroscope. Ring laser gyroscopes are still explored today to describe other phenomena from the Earth's rotation such as the Lense-Thirring Effect, and gyroscopes such as the GINGERino have been proposed to measured such quantities [4].

In our experiment, we use a ring laser gyroscope to attempt to measure the rotation rate of the Earth. This is done by employing the Sagnac effect, which allows us to determine the rotation of an inertial system by the path length difference between two light beams. To observe the quality of the constructed laser gyroscope, we measure optical cavity parameters such as the free spectral range, PDH locking error signals, lock-in threshold, and the finesse. We further quantify the stability and sensitivity

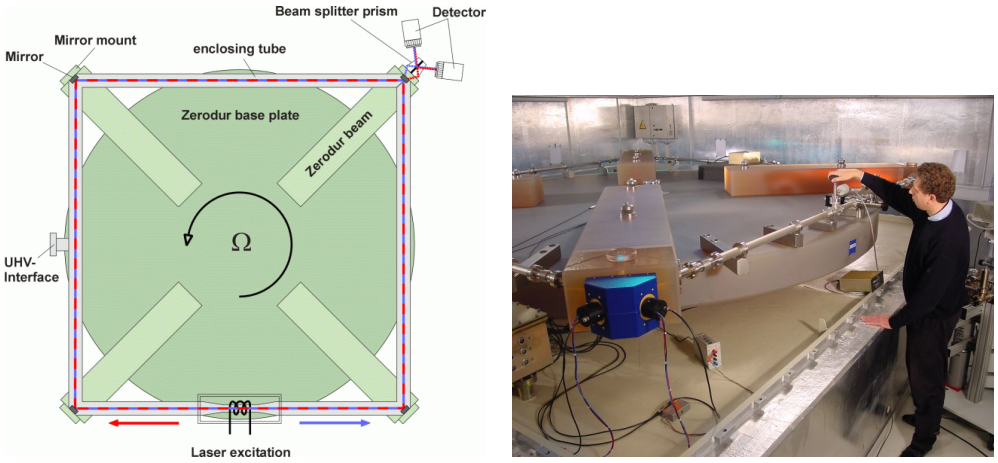

(a) (b)

Figure 1.0.2: The G-Ring gyroscope at the Fundamentalstation Wettzell. (a): The setup of the gyroscope. (b): Image of the G-ring. Obtained from Ref. [3].

of the gyroscope by determining the Allan deviation.

This paper is structured as follows. Chapter 1 motivates the experiment by elaborating on the usage of ring laser gyroscopes to determine the rotation rate of the Earth. Chapter 2 describes the theory behind the quantities measured in the experiment. Chapter 3 describes the setup used in our experiment and the method used to determine the relevant quantities for each part of our experiment. Chapter 4 shows the pre-laboratory tasks that were required before starting the experiment. Chapter 5 shows the results that we have obtained and discussions related to the results. Finally, we summarize our findings and address possible outlooks for our experiment in Chapter 6.

Chapter 2

Theory

2.1 Gyroscopes

2.1.1 The Sagnac Effect

The Sagnac effect tells us that whilst the motion between two inertial frames cannot be distinguished, two rotating frames can be distinguished, allowing one to directly measure the rotation rate of an inertial system [1]. This effect was first observed by George Sagnac in 1913, whom believed that this experiment was a proof that aether exists in an inertial frame [5]. This, however, was disproven by Max von Laue in 1911 where he showed that the Sagnac effect was compatible with special relativity [6]. However, the interpretation of the Sagnac effect due to the general theory of relativity is still investigated today, even though it is already well-known in literature [7]. In our analysis, we utilize the Sagnac effect on a gyroscope to measure the rotation rate of the Earth.

To observe the Sagnac effect, we consider an interferometer setup with light propagating with wavelength λ enclosing an area $\vec{A}$ with perimeter P. Placing such a setup onto a rotating platform with frequency $\vec{\Omega}$, we observe that the optical path that each light travels changes. For example, if the table rotates counter-clockwise, then the path of the co-rotating light increases, while that of the other light decreases (see Fig. 2.1.1). The Sagnac effect then tells us the resulting phase shift between the two lights:

$$\delta\phi = \frac{8\pi\vec{A}\cdot\vec{\Omega}}{c\lambda} \propto \vec{A}\cdot\vec{\Omega} \tag{2.1.1}$$

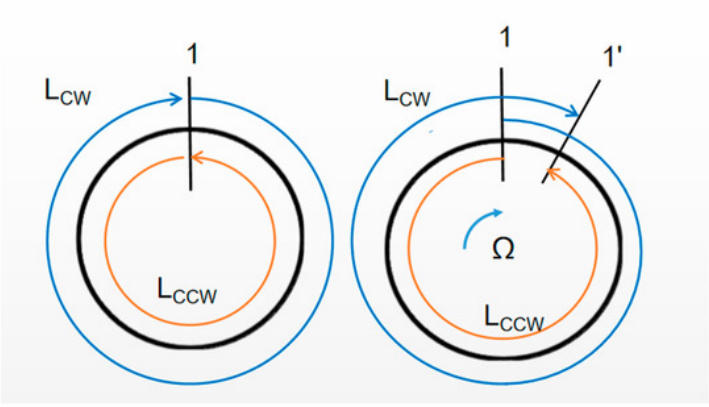

Figure 2.1.1: The Sagnac effect. *Left*: Setup without rotation. The beam moving clockwise (blue) and counter-clockwise (orange) have the same optical path length. *Right*: Setup with a clockwise rotation Ω. The path length of the clockwise beam is larger than that of the counter-clockwise beam. Obtained from Ref. [8].

A more detailed derivation using the relativistic law of velocity addition can be found in Ref. [7].

2.1.2 Ring Laser Gyroscopes

Active Ring Laser Gyroscopes

In order to incorporate the Sagnac effect within our experiment, we utilize ring laser gyroscopes. A laser is placed within an enclosed cavity, and emits two counter-propagating beams. Such beams reflect off mirrors and interfere at the end of their propagation. When rotating the platform in which such setup is placed, different interference patterns can be observed, and transforms the ring cavity system into a cavity resonator. The corresponding beat frequency $\delta\nu$ observed is then the Sagnac frequency, which is given as such:

$$\delta\nu = \frac{4\vec{A}\cdot\vec{\Omega}}{P\lambda} \tag{2.1.2}$$

In our experiment, we only consider square ring cavities so that $A = L^2$ and $P = 4L$, where L is the path length of each arm. As such, we can simplify Eq. 2.1.2 as such:

$$\delta\nu = \frac{L\Omega}{\lambda} = n\Omega \tag{2.1.3}$$

where $n = L/\lambda$ is the number of nodes of the light field in each arm. Thus the Sagnac frequency is proportional to the rotation rate of the inertial system [1].

Passive Ring Laser Gyroscopes

In contrast to the active ring laser gyroscope, in which the laser is contained within the ring cavity, the passive ring laser gyroscope places the laser source outside of the cavity system. In this system, the external laser is locked to the counter-propagating modes of the resonator. By placing the laser outside of the resonator, we can reduce the systematic effects due to the lasing medium and the lock-in effect (see Sec. 2.2.2), and also increase the available light power for the beam. This method, however, also introduces an added complexity of laser locking [1]. See Fig. 2.1.2 for a comparison between the two systems. In our experiment, we use the passive ring laser gyroscope and thus laser locking becomes an importance in our measurements.

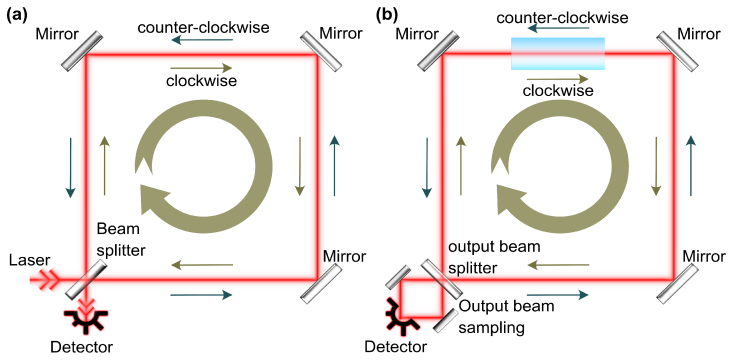

Figure 2.1.2: Ring laser gyroscope systems. *Left*: Passive, *Right*: Active. Obtained from Ref. [9].

Gyroscope Sensitivity

The sensitivity of the ring laser gyroscope depends on a variety of factors, namely the wavelength λ, arm length L, finesse F of the resonator (see Sec. 2.2.1), and the shot-noise limited detection given by the number of photons $N = P_{\text{opt}}/h\nu = P_{\text{opt}}\lambda/hc$ detected per unit time. P_{opt} represents the optical power given to the laser. Combining all such factors, we obtain the sensitivity of the ring laser gyroscope for an integration time τ as such:

$$\delta\Omega = \frac{1}{4}\frac{c}{L^2F}\sqrt{\frac{ch\lambda}{P_{\text{opt}}}}\frac{1}{\sqrt{\tau}} \tag{2.1.4}$$

This gyroscope sensitivity can be directly compared with the Allan deviation σ_{ad} that determines the instability of a measurement for some averaged integration time τ (see Sec. 2.3).

2.2 Optical Cavities

$$\delta\nu_{\mathrm{FSR}} = \frac{c}{P} \tag{2.2.1}$$

2.2.1 Finesse

2.2.2 Lock-In Effect

2.3 Allan Deviation

The Allan deviation is used to quantify the instability of any device that measures differences in frequencies. Assuming that the measurement is only limited by the photon shot-noise (amongst others), we can describe the Allan variance as the deviation between temporal averages of measurements y over some time interval or integration time τ:

$$\sigma_{\mathrm{ad}}^2 = \frac{1}{2M}\sum_{n=1}^{M}(\bar{y}(\tau)_{n+1} - \bar{y}(\tau)_n)^2 \tag{2.3.1}$$

where M is the number of samples. The Allan deviation is then the square root of the variance.

The Allan deviation is especially helpful to understand the sensitivity in gyroscopes. Imposing the same assumptions as above, we can describe the Allan deviation with typical shot noise scaling $\propto 1/\sqrt{\tau}$ as such:

$$\sigma_{\mathrm{ad}} = \frac{\mathcal{A}}{\sqrt{\tau}} \tag{2.3.2}$$

where $\mathcal{A}$ (given in rad/s/$\sqrt{\mathrm{Hz}}$) is known as the sensitivity of the gyroscope. This value can be directly compared with the theoretical gyroscope sensitivity (per integration time) described in Eq. 2.1.4 [1].

Chapter 3

Pre-Lab Exercises

Before conducting the experiment, we were required to determine the rotation rate of the Earth using our phone. Our phones contain a microelectromechanical system (MEMS), which is a portable and inexpensive inertial sensor that track the motion of the phone. Using the application `phyphox` constructed by RWTH Aachen University, we evaluated the capabilities of the MEMS gyroscope within our phones.

3.1 Task 1: Getting Started

3.2 Task 2: Allan Deviation

3.3 Task 3: Rotation Rate of Earth

Chapter 4

Experimental Set-Up and Procedure

4.1 Experimental Set-Up

4.2 Procedure

4.2.1 Free Spectral Range

We first measured both the signal of the laser input and after the laser has passed through the ring cavity system. The window was adjusted until three resonance peaks and their corresponding sidebands were observed. See Fig. 4.2.1 the observed raw signal.

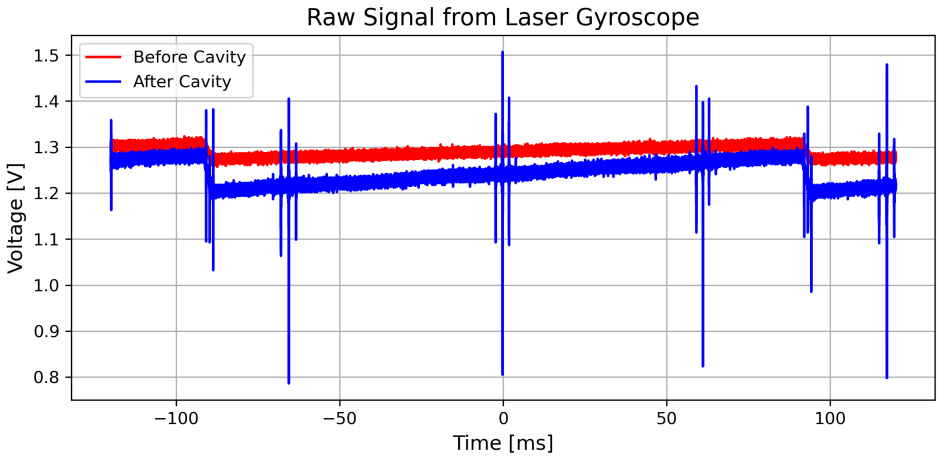

Figure 4.2.1: Raw signal input from the laser before and after passing through the ring cavity system.

As the raw data was provided in the time domain, we converted the time axis into a frequency axis. In order to do so, we use the fact that the modulation frequency from the EOM was $\Omega = 10\,\text{MHz}$, and we determined the width in time between the peaks and the sidebands to obtain a conversion factor between the two axes. From this conversion factor, we obtained the free spectral range as the peak-to-peak difference between the resonance peaks. We also took the average of the values to obtain a mean free spectral range.

We then evaluated the cavity perimeter from Eq. 2.2.1 for each free spectral range that we have observed. We compared our obtained results with the measured value of the cavity perimeter $P_{\text{meas}} = 0.990 \pm 0.005\,\text{m}$ obtained from Ref. [1].

4.2.2 PDH Error Signal

To observe the error signal generated from PDH locking, we observed the combined signal generated from the fast and slow PID controller. Fig. 4.2.2 shows the raw signal obtained from the PDH error. The corresponding data was then used to determine the linear fit of the error signal where the zero crossing

and linear slope is present (i.e. near the middle of the observed error signal). The linear fit was obtained by using `numpy.polyfit`.

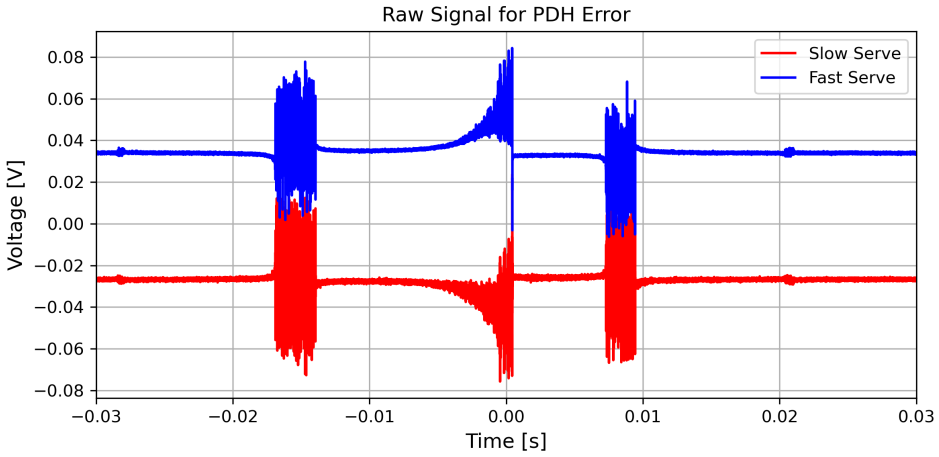

Figure 4.2.2: Raw Signal from PDH locking using the fast and slow PID controller.

The error signal was then used to determine the optimal PID parameters that yield the most stable and large signal. In order to do this, the following parameters were modified: SLOW INT, FAST INT, DIFF GAIN, FAST DIFF / FILTER, SLOW GAIN, FAST GAIN, GAIN LIMIT, and OFFSET. The major parameters that influenced the signal were the SLOW INT, SLOW GAIN, FAST DIFF / FILTER and FAST GAIN. Modifying the SLOW INT and FAST DIFF caused the laser to be out of lock, whereas FAST GAIN decreased the noise observed in the signal. As we decreased the SLOW GAIN, we observed that the laser became more out of lock, allowing for the control of the laser locking. The OFFSET parameter adjusted the offset between the two signals. Table 4.1 shows the optimal PID parameters used in the subsequent measurements which were both stable and yielded a strong signal strength.

PID Parameter	Value
SLOW INT	25
FAST INT	20K
FAST DIFF / FILTER	10M
FAST GAIN	6 dB
GAIN LIMIT	30

Table 4.1: The optimal PID parameters used for this experiment. The SLOW GAIN and FAST GAIN parameter values are not noted as specific values are not marked on the Moglabs PID controller.

When performing laser locking, we further needed to consider the systematics due to the environment. Any small disturbance such as clapping, tapping the desk, moving the cables or even walking influenced the degree of locking for the laser. Other factors such as the temperature fluctuations in the room may have caused the laser to be out of lock as well.

4.2.3 Cavity Ring-Down

4.2.4 Scale Factor

4.2.5 Allan Deviation

Finally, we measured the Allan deviation of the laser gyroscope. We performed the same procedure as with the scale factor measurement. Using the same PID parameters as before, we set the rotation frequency to rotate with 0.75 V, so that the laser will remain locked as long as possible. The gyroscope was rotated until the cable connecting the gyroscope did not extend or contract any further, then the same analysis was performed in the opposite rotation direction. The measurement was taken continuously for approximately 1.5 hours. The unprocessed time series for the frequency measurement can be seen in Fig. 4.2.3.

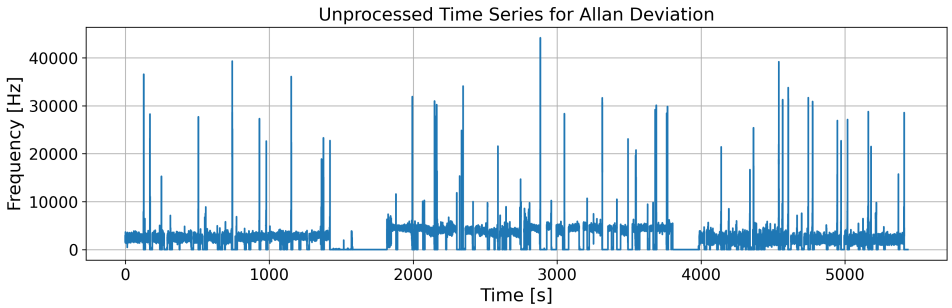

Figure 4.2.3: Unprocessed time series obtained from Allan deviation measurements. We observe large spikes at numerous locations as well as regions with zero frequency.

From the raw data, we first removed any measurements that were taken while the laser was unlocked and when the rotation of the table was switched. After applying some filtering to the data (using `scipy.signal.sosfilt`), we then performed the same procedure as with the Pre-lab tasks in Sec. 3.2 to determine the Allan deviation. We also determined the shot-noise limited time τ by observing the time duration in which the instability of the measurement starts. For the rotation frequency of the table, we followed the same procedure from Sec. 4.2.4.

Chapter 5

Results and Discussion

Chapter 6

Conclusion and Outlook

Chapter 7

Acknowledgements

Bibliography

[1] T. Groh and S. Stellmer, "Laser gyroscope: A249 - course description," Aug. 2021.

[2] D. Behrend, C. Thomas, J. Gipson, E. Himwich, and K. Le Bail, "On the organization of cont17," *Journal of Geodesy*, vol. 94, no. 10, p. 100, Oct. 2020, ISSN: 1432-1394. DOI: 10.1007/s00190-020-01436-x.

[3] F. Wettzell. "Large laser gyroscopes for monitoring earth rotation." (Nov. 2005), [Online]. Available: http://www.fs.wettzell.de/LKREISEL/G/LaserGyros.html (visited on 04/30/2022).

[4] N. Beverini, A. D. Virgilio, J. Belfi, *et al.*, "High-accuracy ring laser gyroscopes: Earth rotation rate and relativistic effects," *Journal of Physics: Conference Series*, vol. 723, p. 012 061, Jun. 2016. DOI: 10.1088/1742-6596/723/1/012061.

[5] O. Darrigol, "Georges sagnac: A life for optics," *Comptes Rendus Physique*, vol. 15, no. 10, pp. 789–840, 2014, The Sagnac effect: 100 years later / L'effet Sagnac : 100 ans après, ISSN: 1631-0705. DOI: https://doi.org/10.1016/j.crhy.2014.09.007.

[6] M. von Laue, "About an experiment on the optics of moving bodies," *Munich session reports 1911*, pp. 405–412, 1911.

[7] E. Benedetto, F. Feleppa, I. Licata, H. Moradpour, and C. Corda, "On the general relativistic framework of the sagnac effect," *The European Physical Journal C*, vol. 79, no. 3, p. 187, Mar. 2019, ISSN: 1434-6052. DOI: 10.1140/epjc/s10052-019-6692-9.

[8] Z. Feng, Y. He, W. Yan, F. Yang, W. Han, and Z. Li, "Progress of waveguide ring resonators used in micro-optical gyroscopes," *Photonics*, vol. 7, no. 4, 2020, ISSN: 2304-6732. DOI: 10.3390/photonics7040096.

[9] I. Kudelin, S. Sugavanam, and M. Chernysheva, "Rotation active sensors based on ultrafast fibre lasers," *Sensors*, vol. 21, no. 10, 2021, ISSN: 1424-8220. DOI: 10.3390/s21103530.

Chapter 8

Appendix